

# Heat transport in magnetic fields by quantum spin liquid in the organic insulators $\text{EtMe}_3\text{Sb}[\text{Pd}(\text{dmit})_2]_2$ and $\kappa - (\text{BEDT} - \text{TTF})_2\text{Cu}_2(\text{CN})_3$

V. R. SHAGINYAN<sup>1,2 (a)</sup>, A. Z. MSEZANE<sup>2</sup>, K. G. POPOV<sup>3</sup>, G. S. JAPARIDZE<sup>2</sup> and V. A. KHODEL<sup>4,5</sup>

<sup>1</sup> *Petersburg Nuclear Physics Institute, Gatchina, 188300, Russia*

<sup>2</sup> *Clark Atlanta University, Atlanta, GA 30314, USA*

<sup>3</sup> *Komi Science Center, Ural Division, RAS, Syktyvkar, 167982, Russia*

<sup>4</sup> *Russian Research Center Kurchatov Institute, Moscow, 123182, Russia*

<sup>5</sup> *McDonnell Center for the Space Sciences & Department of Physics, Washington University, St. Louis, MO 63130, USA*

PACS 75.10.Kt – Quantum spin liquids

PACS 66. – Nonelectronic transport properties of condensed matter

PACS 71.10.Hf – Non-Fermi-liquid ground states

PACS 64.70.Tg – Quantum phase transitions

**Abstract** –Measurements of the low-temperature thermal conductivity collected on insulators with geometrical frustration produce important experimental facts shedding light on the nature of quantum spin liquid composed of spinons. We employ a model of strongly correlated quantum spin liquid located near the fermion condensation phase transition to analyze the exciting measurements of the low-temperature thermal conductivity in magnetic fields collected on the organic insulators  $\text{EtMe}_3\text{Sb}[\text{Pd}(\text{dmit})_2]_2$  and  $\kappa - (\text{BEDT} - \text{TTF})_2\text{Cu}_2(\text{CN})_3$ . Our analysis of the conductivity allows us to reveal a strong dependence of the effective mass of spinons on magnetic fields, to detect a scaling behavior of the conductivity, and to relate it to both the spin-lattice relaxation rate and the magnetoresistivity. Our calculations and observations are in a good agreement with experimental data.

The organic insulators  $\text{EtMe}_3\text{Sb}[\text{Pd}(\text{dmit})_2]_2$  and  $\kappa - (\text{BEDT} - \text{TTF})_2\text{Cu}_2(\text{CN})_3$  have two-dimensional triangular lattices with the geometric frustration prohibiting the formation of spin ordering even at the lowest accessible temperatures  $T$  [1–5]. Therefore, these insulators offer unique insights into the physics of quantum spin liquids (QSL). Indeed, measurements of the heat capacity on the both insulators reveal a  $T$ -linear term indicating that the low-energy excitation spectrum from the ground state is gapless [1–3]. The excitation spectrum can be deduced from measurements of the heat conductivity  $\kappa(T)$  in the low temperature regime. For example, at  $T \rightarrow 0$  a residual value in  $k/T$  signals that the excitation spectrum is gapless. The presence of the residual value is clearly resolved in  $\text{EtMe}_3\text{Sb}[\text{Pd}(\text{dmit})_2]_2$ , while measurements of  $k/T$  on  $\kappa - (\text{BEDT} - \text{TTF})_2\text{Cu}_2(\text{CN})_3$  suggests that the low-energy excitation spectrum can have a gap

[4, 5]. Taking into account the observed  $T$ -linear term of the heat capacity in  $\kappa - (\text{BEDT} - \text{TTF})_2\text{Cu}_2(\text{CN})_3$  with the static spin susceptibility remaining finite down to the lowest measured temperatures [6], the presence of the spin excitation gap becomes questionable. Thermal conductivity probe elementary itinerant excitations and is totally insensitive to localized ones such as those responsible for Schottky contributions, which contaminates the heat capacity measurements at low temperatures [1–5]. The heat conductivity is formed primarily by both acoustic phonons and itinerant spinons, while the latter form QSL. Since the phonon contribution is insensitive to the applied magnetic field  $B$ , the elementary excitations of QSL can be further explored by the magnetic field dependence of  $k$ . Measurements under the application of magnetic field  $B$  of the heat conductivity  $\kappa$  on these insulators have exhibited a strong dependence of  $\kappa(B, T)$  as a function of  $B$  at fixed  $T$  [4, 5]. The obtained dependence at low temperatures re-

<sup>(a)</sup> Email: vrshag@thd.pnpi.spb.ru

sembles that of the spin-lattice relaxation rate ( $1/T_1T$ ) at fixed temperature as a function of magnetic field [7]:  $k(B)$  at low fields is insensitive to  $B$ , displaying a response to increasing magnetic field  $B$ . On the other hand, it is suggested that the observed  $B$ -dependence implies that some spin-gaplike excitations coupling to the magnetic field are also present at low temperatures [4,5]. As a result, we face a challenging problem of interpretation of the experimental data in a consistent way, including the  $B$ -dependence of the heat conductivity.

In this letter we explain the  $B$ -dependence of the low-temperature thermal conductivity  $\kappa$  in  $\text{EtMe}_3\text{Sb}[\text{Pd}(\text{dmit})_2]_2$  and  $\kappa - (\text{BEDT} - \text{TTF})_2\text{Cu}_2(\text{CN})_3$ . We employ a model of strongly correlated quantum spin liquid (SCQSL) located near the fermion condensation phase transition (FCQPT) to analyze the  $B$ -dependence of  $\kappa$  [7–10]. Our analysis allows us to detect a scaling behavior of  $\kappa(B, T)$ , and relate it to the scaling behavior of the spin-lattice relaxation rate ( $1/T_1T$ ) measured on both the herbertsmithite  $\text{ZnCu}_3(\text{OH})_6\text{Cl}_2$  and the heavy-fermion (HF) metal  $\text{YbCu}_{5-x}\text{Au}_x$ , and the magnetoresistivity measured on the HF metal  $\text{YbRh}_2\text{Si}_2$ . Our calculations are in a good agreement with experimental data.

Representing a special case of QSL, SCQSL is a quantum state of matter composed of spinons - chargeless fermionic spinons with spin  $1/2$  [7, 9, 10]. In insulating compounds, SCQSL can emerge when interactions among the magnetic components are incompatible with the underlying crystal geometry, leading to a geometric frustration generated by the triangular and kagome lattices of magnetic moments, as it is in the case of  $\text{ZnCu}_3(\text{OH})_6\text{Cl}_2$ , see e.g. [11–17]. In case of ideal two-dimensional (2D) lattice the frustration of the lattice leads to a dispersionless topologically protected branch of the spectrum with zero excitation energy known as the flat band [18–20]. Then, FCQPT can be considered as quantum critical point of SCQSL, composed of chargeless heavy spinons with  $S = 1/2$  and the effective mass  $M_{\text{mag}}^*$ , occupying the corresponding Fermi sphere with the Fermi momentum  $p_F$ . Therefore, the properties of insulating compounds coincide with those of heavy-fermion metals with one exception: it resists the flow of electric charge [7, 9, 10]. As we are dealing with compounds confining non-ideal triangular and kagome lattices, we have to bear in mind that the real magnetic interactions and possible distortion of the lattices can shift the SCQSL from the exact FCQPT, positioning it somewhere near FCQPT. Therefore, the actual location of the SCQSL phase in fig. 1 has to be established by analyzing the experimental data only.

In the vicinity of the FCQPT, pronounced deviations from the behavior of Landau Fermi liquid (LFL) with regard to physical properties are observed. These so-called non-Fermi-liquid (NFL) phenomena are related to the action of strong enhancement of the effective mass  $M_{\text{mag}}^*$  associated with the FCQPT. We note that there are different kinds of instabilities of LFL connected with several

perturbations of initial quasiparticle spectrum  $\varepsilon(\mathbf{p})$  and occupation numbers  $n(\mathbf{p})$ , associated with strong enhancement of the effective mass and leading to the emergence of a multi-connected Fermi surface, see e.g. [8, 21–23]. Depending on the parameters and analytical properties of the Landau interaction, such instabilities lead to several possible types of restructuring of the initial LFL ground state. This restructuring generates topologically distinct phases. One of them is the fermion condensation associated with FCQPT, another one belongs to a class of topological phase transitions, where the sequence of rectangles  $n(p) = 0$  and  $n(p) = 1$  is realized at  $T = 0$ . In fact, at elevated temperatures the systems located at these transitions exhibit behavior typical to those located at FCQPT [8]. Therefore, we do not consider the specific properties of these topological transitions, and focus on the behavior of systems located near FCQPT.

We start with a brief outline of the effective mass dependence on magnetic field and temperature,  $M_{\text{mag}}^*(B, T)$ . The key point of the formalism is the extended quasiparticle paradigm when the effective mass is no more constant but depends on temperature  $T$ , magnetic field  $B$  and other external parameters such as pressure  $P$  [8]. To study the low temperature transport properties, scaling behavior, and the effective mass  $M_{\text{mag}}^*(B, T)$  of SCQSL, we use the model of homogeneous HF liquid. In that case, the model permits to avoid complications associated with the crystalline anisotropy of solids [8], while the Landau equation, describing the effective mass  $M^*$  of HF liquid, reads [8, 24]

$$\frac{1}{M_{\sigma}^*(B, T)} = \frac{1}{M} + \sum_{\sigma_1} \int \frac{\mathbf{p}_F \mathbf{p}}{p_F^3} F_{\sigma, \sigma_1}(\mathbf{p}_F, \mathbf{p}) \times \frac{\partial n_{\sigma_1}(\mathbf{p}, T, B)}{\partial p} \frac{d\mathbf{p}}{(2\pi)^3}, \quad (1)$$

where  $M$  is the corresponding bare mass,  $F_{\sigma, \sigma_1}(\mathbf{p}_F, \mathbf{p})$  is the Landau interaction, which depends on Fermi momentum  $p_F$ , momentum  $p$  and spin index  $\sigma$ . The distribution function  $n$  can be expressed as

$$n_{\sigma}(\mathbf{p}, T) = \left\{ 1 + \exp \left[ \frac{(\varepsilon(\mathbf{p}, T) - \mu_{\sigma})}{T} \right] \right\}^{-1}, \quad (2)$$

where  $\varepsilon(\mathbf{p}, T)$  is the single-particle spectrum. In our case, the chemical potential  $\mu$  depends on the spin due to Zeeman splitting  $\mu_{\sigma} = \mu \pm \mu_B B$ ,  $\mu_B$  is Bohr magneton.

In LFL theory, the single-particle spectrum is a variational derivative of the system energy  $E[n_{\sigma}(\mathbf{p}, T)]$  with respect to occupation number  $n$ ,  $\varepsilon(\mathbf{p}, T) = \delta E[n(\mathbf{p})]/\delta n$ . Choice of the interaction and its parameters is dictated by the fact that the system has to be at FCQPT [8, 25, 26]. Thus, the sole role of the Landau interaction is to bring the system to the FCQPT point, where Fermi surface alters its topology so that the effective mass acquires temperature and field dependence [8, 23, 25]. The variational procedure, being applied to the functional  $E[n_{\sigma}(\mathbf{p}, T)]$ , gives

the following form for  $\varepsilon_\sigma(\mathbf{p}, T)$ ,

$$\frac{\partial \varepsilon_\sigma(\mathbf{p}, T)}{\partial \mathbf{p}} = \frac{\mathbf{p}}{M} - \sum_{\sigma_1} \int \frac{\partial F_{\sigma, \sigma_1}(\mathbf{p}, \mathbf{p}_1)}{\partial \mathbf{p}} n_{\sigma_1}(\mathbf{p}_1, T) \frac{d^3 p_1}{(2\pi)^3}, \quad (3)$$

Equations (2) and (3) constitute the closed set for self-consistent determination of  $\varepsilon_\sigma(\mathbf{p}, T)$  and  $n_\sigma(\mathbf{p}, T)$  and the effective mass,  $p_F/M_{mag}^* = \partial \varepsilon(p)/\partial(p)|_{p=p_F}$ . We emphasize here, that in our approach the entire temperature and magnetic field dependence of the effective mass is brought to us by dependencies of  $\varepsilon_\sigma(\mathbf{p})$  and  $n_\sigma(\mathbf{p})$  on  $T$  and  $B$ . At FCQPT, eq. (1) can then be solved analytically [8,25]. At  $B = 0$ , the effective mass strongly depends on  $T$  demonstrating the NFL behavior [8,25]

$$M^*(T) \simeq a_T T^{-2/3}. \quad (4)$$

At finite  $T$ , the application of magnetic field  $B$  drives the system to the LFL region with

$$M^*(B) \simeq a_B B^{-2/3}. \quad (5)$$

A deeper insight into the behavior of  $M^*(B, T)$  can be achieved using some "internal" (or natural) scales. Namely, near FCQPT the solutions of eq. (1) exhibit a behavior so that  $M^*(B, T)$  reaches its maximum value  $M_M^*$  at some temperature  $T_M \propto B$  [8]. It is convenient to introduce the internal scales  $M_M^*$  and  $T_M$  to measure the effective mass and temperature. Thus, we divide the effective mass  $M^*$  and the temperature  $T$  by the values,  $M_M^*$  and  $T_M$ , respectively. This generates the normalized effective mass  $M_N^* = M^*/M_M^*$  and the normalized temperature  $T_N = T/T_M$ . Near FCQPT the normalized solution of eq. (1)  $M_N^*(T_N)$  can be well approximated by a simple universal interpolating function [8]. The interpolation occurs between the LFL and NFL regimes and represents the universal scaling behavior of  $M_N^*$  [8]

$$M_N^*(y) \approx c_0 \frac{1 + c_1 y^2}{1 + c_2 y^{8/3}}. \quad (6)$$

Here,  $y = T_N = T/T_M$ ,  $c_0 = (1 + c_2)/(1 + c_1)$ ,  $c_1, c_2$  are fitting parameters. Magnetic field  $B$  enters eq. (1) only in the combination  $\mu_B B/T$ , making  $T_M \sim \mu_B B$ . It follows from eq. (6) that

$$T_M \simeq a_1 \mu_B B, \quad (7)$$

where  $a_1$  is a dimensionless factor. Thus, in the presence of fixed magnetic field the variable  $y$  becomes  $y = T/T_M \sim T/\mu_B B$ . Taking into account eq. (7), we conclude that eq. (6) describes the scaling behavior of the effective mass as a function of  $T$  versus  $B$  - the curves  $M_N^*$  at different magnetic fields  $B$  merge into a single one in terms of the normalized variable  $y = T/T_M$ . Since the variables  $T$  and  $B$  enter symmetrically, eq. (6) describes the scaling behavior of  $M_N^*(B, T)$  as a function of  $B$  versus  $T$ . The normalization procedure deserves a remark here. Namely, since the magnetic field dependence of  $M_N^*(B, T)$  at fixed  $T$  does

not have a maximum, the normalization is performed at its inflection point, occurring at  $B = B_{inf}$ . As a result, we have  $y = B/B_{inf}$  and  $M_N^* = M^*(B, T)/M^*(B_{inf}, T)$ . In other words, the curves  $M_N^*$  at different  $T$  merge into a single one in terms of the normalized variable  $y = B/B_{inf}$ , while eq. (7) transforms into the equation

$$\mu_B B_{inf} \simeq a_2 T, \quad (8)$$

with  $a_2$  is a dimensionless factor.

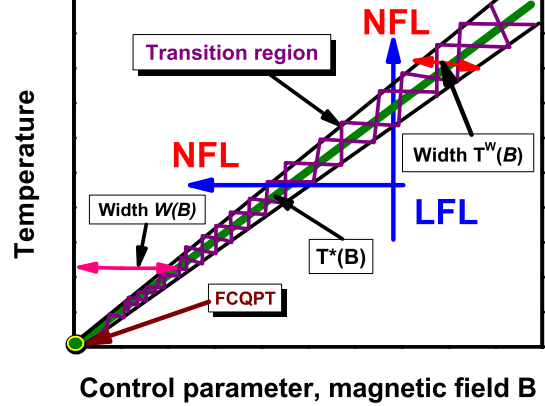


Fig. 1: (Color online). Schematic  $T - B$  phase diagram of SCQSL with magnetic field as the control parameter. The vertical and horizontal arrows show LFL-NFL and NFL-LFL transitions at fixed  $B$  and  $T$ , respectively. The hatched area represents the transition region taking place at  $T^*(B)$ . The solid line in the hatched area represents the function  $T^*(B) \simeq T_M(B)$  given by eq. (7). The functions  $W(B) \propto T \propto T^*$  and  $T^W(B) \propto T \propto T^*$  shown by two-headed arrows define the width of the NFL state and the transition area, respectively. At FCQPT indicated by the arrow the effective mass  $M^*$  diverges and both  $W(B)$  and  $T^W(B)$  tend to zero.

Now we construct the schematic phase diagram of SCQSL of the organic insulators  $\text{EtMe}_3\text{Sb}[\text{Pd}(\text{dmit})_2]_2$  and  $\kappa - (\text{BEDT} - \text{TTF})_2\text{Cu}_2(\text{CN})_3$ . The phase diagram is reported in fig. 1. We assume that at  $T = 0$  and  $B = 0$  the system is approximately located at FCQPT without tuning. Both magnetic field  $B$  and temperature  $T$  play the role of the control parameters, shifting the system from FCQPT and driving it from the NFL to LFL regions as shown by the vertical and horizontal arrows. At fixed temperatures the increase of  $B$  drives the system along the horizontal arrow from the NFL region to LFL one. On the contrary, at fixed magnetic field and increasing temperatures the system transits along the vertical arrow from the LFL region to the NFL one. The hatched area denoting the transition region separates the NFL state from the weakly polarized LFL state and contains the solid line tracing the transition region,  $T^*(B) \simeq T_M(B)$ . Referring to eq. (7), this line is defined by the function  $T^* \propto \mu_B B$ ,

and the width  $W(B)$  of the NFL state is seen to be proportional  $T$ . In the same way, it can be shown that the width  $T^W(B)$  of the transition region is also proportional to  $T$ .

As it was mentioned above, SCQSL plays a role of HF liquid. Thus, we expect that SCQSL in organic insulators behaves like the electronic HF liquid in HF metals, provided that the charge of an electron were zero. In that case, the thermal resistivity  $w$  of SCQSL is related to the thermal conductivity  $\kappa$

$$w = \frac{L_0 T}{\kappa} = w_0 + A_w T^2. \quad (9)$$

In magnetic fields, the resistivity  $w$  behaves like the electrical magnetoresistivity  $\rho_B = \rho_0 + A_\rho T^2$  of the electronic liquid, since  $A_w$  represents the contribution of spinon-spinon scattering to the thermal transport, being analogous to the contribution  $A_\rho$  to the charge transport, defined by electron-electron scattering. Here,  $L_0$  is the Lorenz number,  $\rho_0$  and  $w_0$  are residual resistivity of electronic liquid and QSL, respectively, and the coefficients  $A_w \propto (M_{\text{mag}}^*)^2$  and  $A_\rho \propto (M^*)^2$  [8]. Thus, in the LFL region the coefficient  $A_w$  of the thermal resistivity of SCQSL under the application of magnetic fields at fixed temperature behaves like the spin-lattice relaxation rate shown in fig. 2,  $A_w(B) \propto A_\rho \propto 1/T_1 T(B) \propto (M^*(B)_{\text{mag}})^2$  [26]. In accordance with eq. (5) as seen from fig. 2, panel A, the magnetic field  $B$  progressively reduces  $1/T_1 T$  [27, 28], and  $1/T_1 T$  as a function of  $B$  possesses an inflection point at some  $B = B_{\text{inf}}$  shown by the arrow. The same behavior is seen from fig. 2, the panel B: The magnetic field  $B$  diminishes the longitudinal magnetoresistivity [29], and it as a function of  $B$  possesses an inflection point shown by the arrow. This behavior is consistent with the phase diagram displayed in fig. 1: At growing magnetic fields the NFL behavior first converts into the transition one and then transforms into the LFL behavior.

Figure 2, panels A and B, display the normalized spin-lattice relaxation rates  $(1/T_1 T)_N$  and the longitudinal magnetoresistivity  $\rho_B$  at fixed temperature versus normalized magnetic field  $B_N$ , correspondingly. To clarify the universal scaling behavior of the herbertsmithite and the HF metal  $\text{YbCu}_{5-x}\text{Au}_x$ , we normalize both the functions  $1/T_1 T$  and  $(\rho_B - \rho_0)$  and the magnetic field. Namely, we normalize the functions by their values at the inflection point, and magnetic field is normalized by  $B_{\text{inf}}$ ,  $B_N = B/B_{\text{inf}}$ . Since  $(1/T_1 T)_N = \rho_B - \rho_0 = (M_N^*(B))^2$  [8, 26], we expect that the different strongly correlated Fermi systems located near FCQPT exhibit the same behavior of the effective mass, as it is seen from fig. 2, panels A and B. We shall see below that the heat conductivity of the organic insulators exhibits the same behavior.

Study of the thermal resistivity  $w$  given by eq. (9) allows one to reveal spinons as itinerant excitations. It is important that  $w$  is not contaminated by contributions coming from localized excitations. The temperature dependence of thermal resistivity  $w$  represented by the finite term  $w_0$

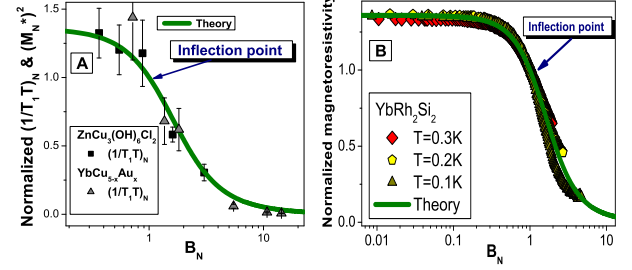


Fig. 2: (Color online). Panel A. The relaxation properties of the herbertsmithite versus those of HF metals. The normalized spin-lattice relaxation rate  $(1/T_1 T)_N$  at fixed temperature as a function of magnetic field: Squares correspond to data on  $(1/T_1 T)_N$  extracted from measurements on  $\text{ZnCu}_3(\text{OH})_6\text{Cl}_2$  [27], while the triangles correspond to those extracted from measurements on  $\text{YbCu}_{5-x}\text{Au}_x$  with  $x = 0.4$  [28]. The inflection point, representing the transition region, where the normalization is taken is shown by the arrow. Our calculations based on eqs. (1) and eq. (6) are depicted by the solid curve, tracing the scaling behavior of  $(M_N^*)^2$  and representing the  $B$ -dependence of the thermal resistivity  $w$ , see main text and eq. (9). Panel B. The normalized longitudinal magnetoresistivity  $\rho_N$  versus  $B_N$ ,  $\rho_N$  is extracted from measurements on  $\text{YbRh}_2\text{Si}_2$  at different temperatures [29] listed in the legend. The solid curve represents our calculations of  $(M_N^*)^2$ .

directly shows that the behavior of SCQSL is similar to that of metals, and there is a finite residual term  $\kappa/T$  in the zero-temperature limit of  $\kappa$ . The presence of this term immediately proves that there are gapless excitation associated with the property of normal and HF metals, in which gapless electrons govern the heat and charge transport, revealing a connection between the classical physics and quantum criticality [30]. The finite  $w_0$  means that in QSL both  $k/T$  and  $C_{\text{mag}}/T \propto M_{\text{mag}}^*$  remain nonzero at  $T \rightarrow 0$ . Therefore, gapless spinons, forming the Fermi surface, govern the specific heat and the transport. Key information on the nature of spinons is further provided by the  $B$ -dependence of the coefficient  $A_w$ . The specific  $B$ -dependence of  $(1/T_1 T)_N \propto (M_{\text{mag}}^*)^2$ , shown in fig. 2, panel A, and given by eq. (5), establishes the behavior of QSL as SCQSL. We note that the heat transport is polluted by the phonon contribution. On the other hand, the phonon contribution is hardly influenced by the magnetic field  $B$ . Therefore, we expect the  $B$ -dependence of the heat conductivity to be governed by  $A_w(B, T)$ . Consider the approximate relation,

$$1 - \frac{A_w(B, T)}{A_w(0, T)} = 1 - \left( \frac{M^*(B, T)_{\text{mag}}}{M^*(0, T)_{\text{mag}}} \right)^2 \simeq a(T) \frac{\kappa(B, T) - \kappa(0, T)}{\kappa(0, T)} \equiv a(T) I(B, T), \quad (10)$$

where the coefficient  $a(T)$  is  $B$ -independent. To derive



(10), we employ eq. (9), and obtain

$$\frac{\kappa}{L_0 T} = \frac{1}{w_0 + A_w T^2} + b T^2. \quad (11)$$

Here, the term  $bT^2$  describes the phonon contribution to the heat transport. Upon carrying out simple algebra and assuming that  $[1 - A_w(B, T)/A_w(0, T)] < 1$ , we arrive at eq. (10). It is seen from fig. 2, the both panels, that the effective mass  $M_N^*(B) \propto M_{\text{mag}}^*(B)$  is a diminishing function of magnetic field  $B$ . Then, it follows from eqs. (5), (6) and (10) that the function  $I(B, T) = [\kappa(B, T) - \kappa(0, T)]/\kappa(0, T)$  increases at elevated field  $B$  in the LFL region, while  $I(B, T) \simeq 0$  in the NFL region, for the function is approximately independent of  $B$  in that case.

Recent measurements of  $\kappa(B)$  on the organic insulators  $\text{EtMe}_3\text{Sb}[\text{Pd}(\text{dmit})_2]_2$  and  $\kappa - (\text{BEDT} - \text{TTF})_2\text{Cu}_2(\text{CN})_3$  [4, 5] are displayed in figs. 3 and 4, panels A. The measurements show that the heat is carried by phonons and SCQSL, for the heat conductivity is well fitted by  $\kappa/T = b_1 + b_2 T^2$ , where  $b_1$  and  $b_2$  are constants. The finite  $b_1$  term implies that spinon excitations are gapless in  $\text{EtMe}_3\text{Sb}[\text{Pd}(\text{dmit})_2]_2$ , while in  $\kappa - \text{BEDT} - \text{TTF})_2\text{Cu}_2(\text{CN})_3$  gapless excitations are under debate [5]. A simple estimation indicates that the ballistic propagation of spinons seems to be realized in the case of  $\text{EtMe}_3\text{Sb}[\text{Pd}(\text{dmit})_2]_2$  [4, 5]. It is seen from figs. 3 and 4, panels A, that  $I(B, T) = [\kappa(B, T) - \kappa(B = 0, T)]/\kappa(B = 0, T)$  demonstrates a strong  $B$ -dependence, namely the field dependence shows an increase of thermal conductivity for rising fields  $B$ . Such a behavior is in agreement with eq. (5) and fig. 2 which demonstrate that  $(M_{\text{mag}}^*(B))^2$  is a diminishing function of  $B$ . As a result, it follows from eq. (10) that  $I(B, T)$  is an increasing function of  $B$ . Our calculations based on eqs. (3) and (10) are depicted by geometrical figures in figs. 3 and 4, panels A. Since we cannot calculate the parameter  $a(T)$  entering eq. (10) we use it as a fitting parameter. Temperature  $T$  was also used to fit the data at temperatures shown in the legend in figs. 3 and 4. It is seen from figs. 3 and 4, panels A, that  $I(B, T)$  as a function of  $B$  possesses an inflection point at some  $B = B_{\text{inf}}$ . To reveal the scaling behavior of the heat conductivity of the organic insulators, we normalize both the function  $I(B, T)$  and the magnetic field by their values at the inflection points, as it was done in the case of  $(1/T_1 T)_N$ , see fig. 2. The normalized heat conductivity  $I_N(B_N, T)$  does not depend on the factor  $a(T)$ , entering eq. (10), and its calculations do not have any fitting parameters. It is seen from figs. 3 and 4, panels B, that in accordance with eq. (6)  $I_N(B_N, T)$  exhibits the scaling behavior and becomes a function of a single variable  $B_N$ . It is instructive to compare the normalized values of the function  $(1 - 1/T_1 T)_N \equiv (1 - [M^*(B, T)/M^*(B = 0, T)]^2)_N$  extracted from measurements of  $(1/T_1 T)_N$  shown in fig. 2, panel A, with  $I_N(B_N, T)$ . The extracted values are normalized by their values at the inflection points and magnetic field is normalized by  $B_{\text{inf}}$ , as it is done in the

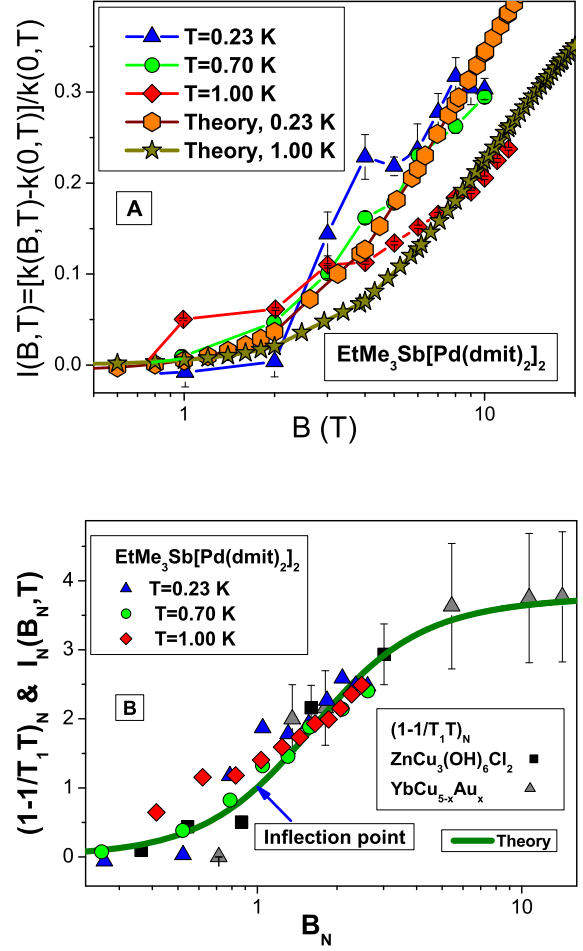


Fig. 3: (Color online). Panel A: Magnetic field  $B$  dependence of the thermal conductivity  $I(B, T)$  measured on the organic insulator  $\text{EtMe}_3\text{Sb}[\text{Pd}(\text{dmit})_2]_2$  and standardized by the zero field value  $\kappa$ ,  $I(B, T) = [\kappa(B, T) - \kappa(B = 0, T)]/\kappa(B = 0, T)$  at temperatures shown in the legend [4, 5]. Our calculations are based on eq. (10) and shown by pentagons and stars. Panel B: The normalized thermal conductivity  $I_N(B_N, T)$  versus  $B_N$  shown by geometrical figures is extracted from the data shown in the panel A of this figure. The inflection point is shown by the arrow. The magnetic field dependence of the function  $(1 - 1/T_1 T)_N$  is extracted from measurements of  $(1/T_1 T)_N$  shown in fig. 2, panel A. The solid curve is obtained from the theoretical curve in fig. 2.

case of  $(1/T_1 T)_N$ . It is seen from figs. 3 and 4, panels B, that  $(1 - 1/T_1 T)_N$  and  $I_N(B_N, T)$  are in good overall agreement with the solid curve depicting the theoretical function  $(1 - [M^*(B, T)/M^*(B = 0, T)]^2)_N$ , received from our calculations represented by the solid curve in fig. 2, the both panels. It is seen that this function demonstrates a flat dependence at low  $B_N$ , for at  $B_N < 1$  the system is in its NFL state and the  $B$ -dependence is weak. Thus, there is no need to introduce additional quasiparticles activated by the application of magnetic field in order to explain

the growth of  $I(B, T)$  at elevated  $B$  [4, 5]. It is also seen from both figs. 3 and 4, panels **B**, the organic insulators demonstrate the same behavior as  $\text{ZnCu}_3(\text{OH})_6\text{Cl}_2$ ,  $\text{YbCu}_{5-x}\text{Au}_x$ , and  $\text{YbRh}_2\text{Si}_2$ .

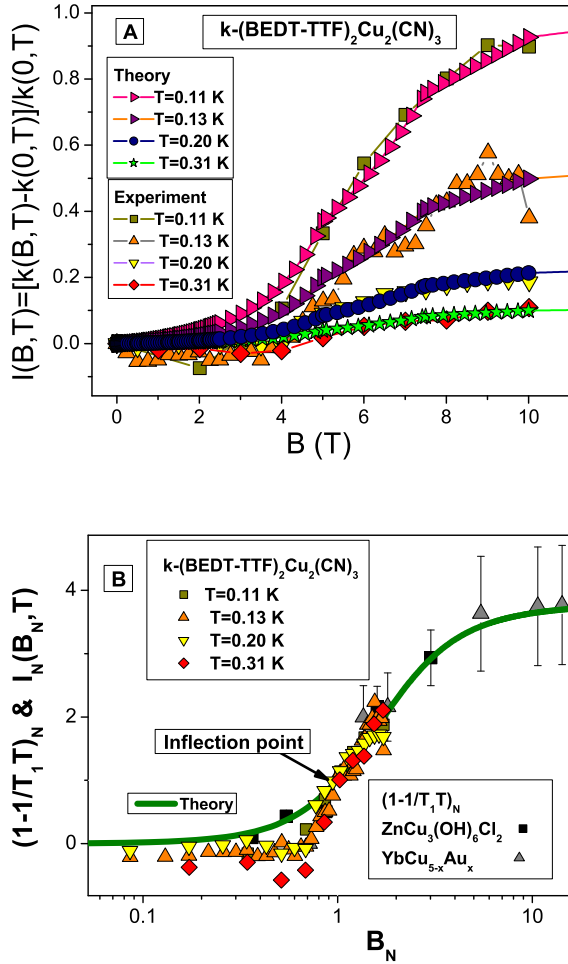


Fig. 4: (Color online). Panel **A**: Magnetic field  $B$  dependence of the thermal conductivity  $I(B, T)$  measured on the organic insulator  $\kappa - (\text{BEDT} - \text{TTF})_2\text{Cu}_2(\text{CN})_3$  and standardized by the zero field value  $\kappa$ ,  $I(B, T) = [\kappa(B, T) - \kappa(B = 0, T)]/\kappa(B = 0, T)$  at temperatures shown in the legend [5]. Our calculations are based on eq. (10) and the results are shown by geometrical figures as displayed in the legend. Panel **B**:  $I_N(B_N, T)$  versus  $B_N$  shown by geometrical figures is extracted from the data shown in the panel **A**, of this figure. The magnetic field dependence of the function  $(1 - 1/T_1T)_N$  is extracted from measurements of  $(1/T_1T)_N$  shown in fig. 2, panel **A**. The solid curve is obtained from the theoretical curve in fig. 2.

In summary, for the first time, we have explained magnetic field-dependence of the low-temperature thermal conductivity  $\kappa$  in the organic insulators  $\text{EtMe}_3\text{Sb}[\text{Pd}(\text{dmit})_2]_2$  and  $\kappa - (\text{BEDT} - \text{TTF})_2\text{Cu}_2(\text{CN})_3$ . Our analysis allows us to detect SCQSL in these organic insulators, exhibiting the universal scaling behavior.

This work was supported by U.S. DOE, Division of

Chemical Sciences, Office of Basic Energy Sciences, Office of Energy Research, AFOSR, and U.S ARO (Grant W911NF-11-1-0194).

## REFERENCES

- [1] YAMASHITA S. *et al.*, *Nat. Phys.*, **4** (2008) 459.
- [2] YAMASHITA M. *et al.*, *Nat. Phys.*, **5** (2009) 44.
- [3] YAMASHITA S. *et al.*, *Nat. Commun.*, **2** (2011) 275.
- [4] YAMAMOTO H. M. *et al.*, *Science*, **328** (2010) 1246.
- [5] YAMASHITA M., SHIBAUCHI T. and MATSUDA Y., *ChemPhysChem*, **13** (2012) 74.
- [6] SHIMIZU Y. *et al.*, *Phys. Rev. Lett.*, **91** (2003) 107001.
- [7] SHAGINYAN V. R. *et al.*, *Europhys. Lett.*, **97** (2012) 56001.
- [8] SHAGINYAN V. R., AMUSIA M. YA., MSEZANE A. Z. and POPOV K. G., *Phys. Rep.*, **492** (2010) 31.
- [9] SHAGINYAN V. R., MSEZANE A. Z. and POPOV K. G., *Phys. Rev. B*, **84** (2011) 060401(R).
- [10] SHAGINYAN V. R., MSEZANE A. Z., POPOV K. G. and KOHDEL V. A., *Phys. Lett. A*, **376** (2012) 2622.
- [11] HAN T.-H. *et al.*, *Nature*, **492** (2012) 406.
- [12] BALENTS L., *Nature*, **464** (2010) 199.
- [13] HELTON J. S. *et al.*, *Phys. Rev. Lett.*, **98** (2007) 107204.
- [14] DE VRIES M. A. *et al.*, *Phys. Rev. Lett.*, **100** (2008) 157205.
- [15] HELTON J. S. *et al.*, *Phys. Rev. Lett.*, **104** (2010) 147201.
- [16] HAN T. H., CHU S. and LEE Y. S., *Phys. Rev. Lett.*, **108** (2012) 157202.
- [17] BERT F. and MENDELS P., *J. Phys. Soc. Jpn.*, **79** (2010) 011001.
- [18] GREEN D., SANTOS L. and CHAMON C., *Phys. Rev. B*, **82** (2010) 075104.
- [19] HEIKKILÄ T. T., KOPNIN N. B. and VOLOVIK G. E., *JETP Lett.*, **94** (2011) 233.
- [20] KOPNIN N. B., HEIKKILÄ T. T. and VOLOVIK G. E., *Phys. Rev. B*, **83** (2011) 220503(R).
- [21] ARTAMONOV S. A., POGORELOV YU. G. and SHAGINYAN V. R., *JETP Lett.*, **68** (1998) 942.
- [22] ZVEREV M. V. and BALDO M., *JETP*, **87** (1998) 1129.
- [23] KHODEL V. A., CLARK J. W. and ZVEREV M. V., *Phys. Rev. B*, **78** (2008) 075120.
- [24] LANDAU L. D., *Sov. Phys. JETP*, **3** (1956) 920.
- [25] CLARK J. W., KHODEL V. A. and ZVEREV M. V., *Phys. Rev. B*, **71** (2005) 012401.
- [26] SHAGINYAN V. R. *et al.*, *Europhys. Lett.*, **93** (2011) 17008.
- [27] IMAI T. *et al.*, *Phys. Rev. Lett.*, **100** (2008) 077203.
- [28] CARRETTA P., PASERO R., GIOVANNINI M. and BAINES C., *Phys. Rev. B*, **79** (2009) 020401(R).
- [29] GEGENWART P. *et al.*, *Science*, **315** (2007) 969.
- [30] SHAGINYAN V. R., POPOV K. G. and KOHDEL V. A., *Phys. Rev. B*, **88** (2013) 115103.